Engineering 6 (2020) 119–131

Contents lists available at ScienceDirect

Engineering

journal homepage: www.elsevier.com/locate/eng

Research
Rare Earth Permanent Magnets—Review

Perspective and Prospects for Rare Earth Permanent Magnets

J.M.D. Coey [a,b]

[a] School of Physics & Centre for Research on Adaptive Nanostructures and Nanodevices, Trinity College Dublin, Dublin 2, Ireland
[b] Department of Materials Science, Beihang University, Beijing 100191, China

ARTICLE INFO

Article history:
Received 7 August 2018
Revised 19 September 2018
Accepted 12 November 2018
Available online 19 June 2019

Keywords:
Rare earth magnets
Magnetic anisotropy
Coercivity
Energy product
Magnetic composites
Additive manufacturing

ABSTRACT

Rare earth permanent magnets constitute a mature technology, but the shock of the 2011 rare earth crisis led to the re-evaluation of many ideas from the 1980s and 1990s about possible new hard magnets containing little or no rare earth (or heavy rare earth). Nd–Fe–B magnets have been painstakingly and skillfully optimized for a wide range of applications in which high performance is required at reasonable cost. Sm–Co is the material of choice when high-temperature stability is required, and Sm–Fe–N magnets are making their way into some niche applications. The scope for improvement in these basic materials by substitution has been rather thoroughly explored, and the effects of processing techniques on the microstructure and hysteresis are largely understood. A big idea from a generation ago—which held real potential to raise the record energy product significantly—was the oriented exchange-spring hard/soft nanocomposite magnet; however, it has proved very difficult to realize. Nevertheless, the field has evolved, and innovation has flourished in other areas. For example, electrical personal transport has progressed from millions of electric bicycles to the point where cars and trucks with electrical drives are becoming mainstream, and looks ready to bring the dominance of the internal combustion engine to an end. As the limitations of particular permanent magnets become clearer, ingenuity and imagination are being used to design around them, and to exploit the available mix of rare earth resources most efficiently. Huge new markets in robotics beckon, and the opportunities offered by additive manufacturing are just beginning to be explored. New methods of increasing magnet stability at elevated temperature are being developed, and integrated multifunctionality of hard magnets with other useful properties is now envisaged. These themes are elaborated here, with various examples.

1. Introduction

The attraction at a distance of ferrous objects to a permanent magnet has been a source of curiosity to children and initiates alike ever since the Iron Age. The first magnets were naturally magnetized iron-oxide-rich rocks. Later investigations of magnetic phenomena, and especially of the directional property, led to the invention of steel wire magnets for compasses in the 11th century, and steel bar and horseshoe magnets in the 18th century. These permanent magnets played a minor role in the electromagnetic revolution of the 19th century (by then, electromagnets were a better way to generate a magnetic field), but steel wire was the medium used in the first demonstration of magnetic recording [1].

A series of practical innovations in the 20th century—most notably, the discovery and development of new materials with sufficient anisotropy to retain their magnetization no matter what their shape—marked the beginning of a revolution in permanent magnet technology that is still gathering pace. A milestone was the discovery of new alloys of a rare earth element with ferromagnetic cobalt (Co) or iron (Fe). These rare earth permanent magnets now create the magnetic field needed for countless practical applications. Energy is stored in the "stray" field that magnets generate in their vicinity. The amount of energy is not large—there is more chemical energy available from a grain of rice than magnetic energy stored in the stray field created by a kilogram of the best Nd–Fe–B (~50 J)—but the magnetic field requires no continuous expenditure of energy, and the energy associated with the field is undiminished by use. This article provides an account of the current status of rare earth permanent magnets, and looks at their future prospects. The reader can find several other recent reviews on this topic [2–4], and there is a new two-volume monograph on rare earth permanent magnet materials in Chinese [5].

E-mail address: jcoey@tcd.ie

https://doi.org/10.1016/j.eng.2018.11.034

1.1. Scientific background

Magnetization $\boldsymbol{M}$ is the key quantity to consider in a ferromagnet. Defined as the magnetic moment $\boldsymbol{m}$ in A·m^2 per unit magnet volume, it has the units of A·m^{-1}, which are the same as the unit of magnetic field strength, $\boldsymbol{H}$. Three intrinsic magnetic properties of a magnetic material are its Curie temperature T_C, its saturation magnetization when fully magnetized $\boldsymbol{M}_s$, and the leading term in the expansion of the uniaxial anisotropy energy K_u, which is usually of magnetocrystalline origin. Rare earth permanent magnet materials have a uniaxial crystal structure—whether tetragonal, hexagonal, or rhombohedral—and the magnetization prefers to lie along the crystallographic symmetry axis. Deviation of the magnetization vector from the easy axis by an angle θ increases the energy by

$$E_a = K_u \sin^2\theta \tag{1}$$

where K_u is positive and of the order 1 MJ·m^{-3}. Magnetization of a ferromagnet tends to be reduced by domain formation; however, the saturation magnetization $\boldsymbol{M}_s$ is the maximum value of remanence possible for a fully magnetized single-domain specimen. Such a fully magnetized state is *metastable*, precisely because the stray field $\boldsymbol{H}$ in the space surrounding the magnet is associated with a positive energy density $(1/2)\mu_0 H^2$. As mentioned earlier, the H field has the units A·m^{-1}, and the magnetic constant μ_0 is $4\pi \times 10^{-7}$ J·(A^2·m)$^{-1}$ (equivalent to T·m·A^{-1} or H·m^{-1} where H is the symbol for henry, the unit of inductance) [6].

An identity in electromagnetism is $\int \boldsymbol{B}\cdot\boldsymbol{H}\mathrm{d}V = 0$, where d$V$ is a volume element and where the integral is over all space. If space is divided into the region outside the magnet, index e, where $\boldsymbol{B} = \mu_0\boldsymbol{H}$, and the region occupied by the magnet itself, index i, where $\boldsymbol{B} = \mu_0(\boldsymbol{H} + \boldsymbol{M})$, we find:

$$-\int_i \boldsymbol{B}\cdot\boldsymbol{H}\mathrm{d}V = \int_e \boldsymbol{B}\cdot\boldsymbol{H}\mathrm{d}V = \int_e \mu_0 H^2 \mathrm{d}V \tag{2}$$

The integral on the left, known as the energy product, is the integral over the magnet volume of the magnetic flux density $\boldsymbol{B}$ and the negative of the $\boldsymbol{H}$ field created by the magnet on itself, which is known as the demagnetizing field $\boldsymbol{H}_d$. The energy product is equal to twice the energy associated with the stray field created by the magnet in the surrounding space. The energy product should be as large as possible. It depends on the magnet shape and the form of the second-quadrant hysteresis loop $B(H)$, where H is the internal field. The maximum energy product $(-BH)_{max}$ is the figure of merit used to characterize a particular grade of permanent magnet material. It is equal to the area of the biggest rectangle that can be inscribed in the second quadrant of the $B(H)$ hysteresis loop. (The minus sign is conventionally omitted.)

In general, the remanence $B_r \le \mu_0 M_s$—the equality applies only for an ideally square $M(H)$ hysteresis loop (Fig. 1(a))—and the demagnetizing field is spatially non-uniform within the magnet, depending on the magnet shape. However, for magnets with an ellipsoidal shape only, the demagnetizing field is given by the following:

$$\boldsymbol{H}_d = -N_i\boldsymbol{M} \tag{3}$$

where $\boldsymbol{M}$ lies along a principal axis (x, y, or z) and N_i is the corresponding demagnetizing factor. Another result from micromagnetic theory [7] is that $N_x + N_y + N_z = 1$, so that the demagnetizing factor for a sphere, for example, is 1/3. It is zero for a long needle-shaped ellipsoid or for a toroid magnetized around the axis. For the ellipsoid, $\boldsymbol{H}$ and $\boldsymbol{M}$ are parallel, and the first integral in Eq. (1) becomes $-\mu_0(H_d + M)H\mathrm{d}V = \mu_0 M^2(N - N^2)V$. This energy is at the maximum when $N = 1/2$ a shape illustrated in Fig. 2. More generally, N_{ij} is a second-order tensor. The *upper limit* on the energy product per unit volume for a magnet grade with an ideal square loop having $M = M_s$ is therefore $(-BH)_{MAX} = (1/4)\mu_0 M_s^2$, since $N = 1/2$. The energy product can never exceed this value. The load line $B = \mu_0(1 - 1/N)H$ lies in the second quadrant (Fig. 1(c)), and cuts the $B(H)$ curve at the working point.

Whenever possible, it is best to measure $(BH)_{max}$ in a closed circuit with the magnet clamped between the pole faces of an electromagnet, in a toroidal geometry where $N \approx 0$.

The demagnetizing field is only uniform for an ellipsoid. Practical magnets never have such a shape. Most common shapes are circular cylinders or rectangular blocks, where $\boldsymbol{H}_d$ is far from uniform, especially at the pole surfaces normal to $\langle\boldsymbol{M}\rangle$ and at the edges and corners of these surfaces. The local magnitude of $\boldsymbol{H}_d$ can be much larger than its value at the center of the magnet, as illustrated in Fig. 2, and the direction can be different to that of $\langle\boldsymbol{M}\rangle$.

There are two consequences of the non-uniform demagnetizing field: The first is that magnetization reversal is generally nucleated at the edges and corners, where the component of the $\boldsymbol{H}$ field directed oppositely to $\boldsymbol{M}$ is greatest; and the second is that the direction of magnetization there deviates from the magnetic axis of the magnet by an angle that depends on K_u.

Since the perpendicular component of the magnetic flux density $\boldsymbol{B}$ is continuous at any interface and $\boldsymbol{B} = \mu_0(\boldsymbol{H} + \boldsymbol{M})$, it follows that $\boldsymbol{H}$ is discontinuous. The surface of the magnet, as well as the zone below it where $\nabla\cdot\boldsymbol{M} \neq 0$, is the source of the $\boldsymbol{H}$ field, which may be represented by a distribution of magnetic "charge" of negative and positive sign or, more traditionally, by a distribution of

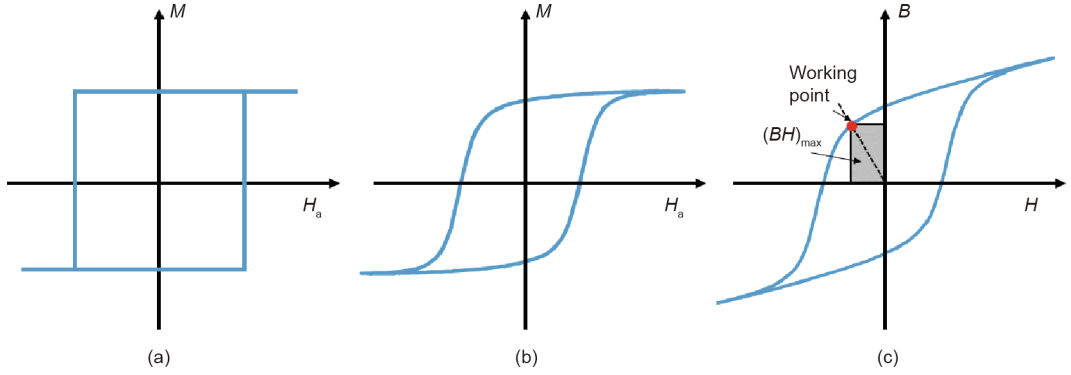

Fig. 1. (a) Ideal and (b) realistic $M(H_a)$ hysteresis loops of a hard magnetic material, where H_a is the externally applied field; (c) the $B(H)$ loop of a permanent magnet where H is the internal field acting on the magnet. The load line (dashed), working point, and energy product (given by the area of the shaded rectangle) all depend on the magnet shape.

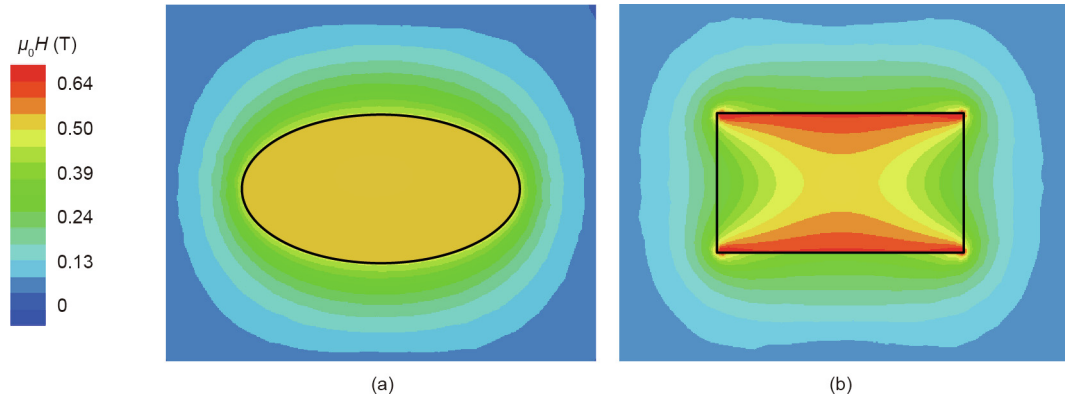

Fig. 2. Illustration of the magnitude of H (a) for an ellipsoid and (b) for an ideal, uniformly magnetized cylinder, both with $N = 1/2$ and $\mu_0 M = 1$ T. The demagnetizing field is uniform in the ellipse, but highly non-uniform in the cylinder, where it is stronger than −0.6 T at the flat surfaces and edges.

magnetic north and south "poles." Isolated, uncompensated magnetic charge or poles do not exist in nature. Nevertheless, as a mathematical fiction, they are useful for envisaging common situations in micromagnetics.

Practical rare earth permanent magnets take one of four forms, as illustrated in Fig. 3 and Table 1. The better ones have higher magnetization $\langle \boldsymbol{M} \rangle$, averaged over the whole volume of rare earth magnetic material and binder phases. The energy product scales as $\langle \boldsymbol{M} \rangle^2$, so the best magnets have highly oriented grains of the rare earth magnet phase and the minimum volume $(1 - f)$ of nonmagnetic intergranular or binder material. Unfortunately, homogeneous single crystals, which are perfectly oriented with a fill factor $f = 1$, are of no use because they exhibit little or no coercivity; magnetization reversal at a single point spreads rapidly to infect the whole crystal. The best sintered magnets have highly oriented small magnetic grains, and only a few percent nonmagnetic binder. Next in efficacy are the oriented, bonded magnets manufactured by compression or injection molding; in these, the magnetic grains are embedded in a polymer matrix with $1 - f \approx 0.3$. Therefore the energy product is about half that of a fully dense oriented, sintered magnets. Magnets made from randomly oriented grains are worse. If a single grain has a square loop with magnetization $\boldsymbol{M}_s$, a fully dense collection of non-interacting, randomly oriented grains magnetized in the easy direction closest to a field applied in the z direction has $\langle M_z \rangle = (1/2)M_s$; hence, the energy product is reduced by a factor of four relative to a dense sintered magnet. In practice, magnets may perform somewhat better than this random-orientation estimate because intergranular interactions can lead to an enhancement of the remanence to a value somewhat greater than $(1/2)M_s$. Worst of all are the randomly oriented, bonded magnets that yield energy products eight times less than the best oriented magnet while using 70% hard magnetic material—an efficiency of just 18%. In practice, the benefits of the alignment of costly rare earth magnet material normally justify the costs of this process step. Cheap, randomly oriented bonded ferrite material finds a low-end market, but for certain applications such as spindle motors for hard disc drives, the benefits of mechanical strength and precise dimensional tolerances, along with the possibility of magnetization in any desired direction, outweigh the low flux density of bonded, isotropic Nd–Fe–B. Table 1 compares the ideal performance of the different magnet grades.

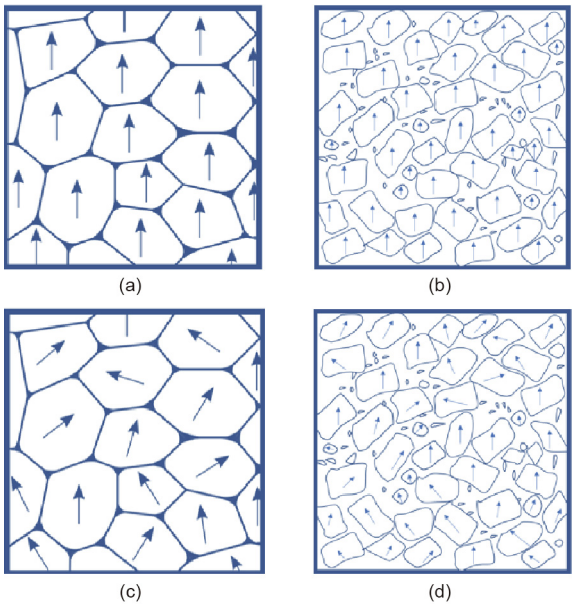

Fig. 3. Possible forms of rare earth permanent magnets. (a) Oriented, sintered magnet; (b) oriented, bonded magnet; (c) random, sintered magnet; (d) random, bonded magnet.

Table 1
Energy products of ideal oriented or random, sintered, or bonded magnets made from $Nd_2Fe_{14}B$ having $M_s = 1.28$ MA·m^{-1}.

Magnet	Energy product	$(BH)_{max}$ (kJ·m^{-3})	Efficiency (%)
Oriented, sintered	$(1/4)\mu_0 M_s^2$	515	100
Oriented, bonded	$(1/4)f^2\mu_0 M_s^2$	252	70
Random, sintered	$(1/16)\mu_0 M_s^2$	129	25
Random, bonded	$(1/16)f^2\mu_0 M_s^2$	63	18

The fill factor f for bonded magnets is taken as 0.7.

1.2. Economic background

Permanent magnets are bulk functional magnetic materials, and their development in recent decades has been strongly influenced by raw materials costs. Although almost any element can be used to make thin-film devices—whether gold for electrical contacts, platinum alloys for recording media, ruthenium for spacer or seed layers, or iridium alloys for exchange bias—these metals cannot be envisaged for use in permanent magnets; they are too expensive. Fig. 4 shows an updated cost periodic table [8]. The choice of materials for permanent magnets is restricted to the first three cost categories (colored blue, yellow, and pink in the figure), although only small amounts of elements in the third category, such as Dy or Tb, are acceptable.

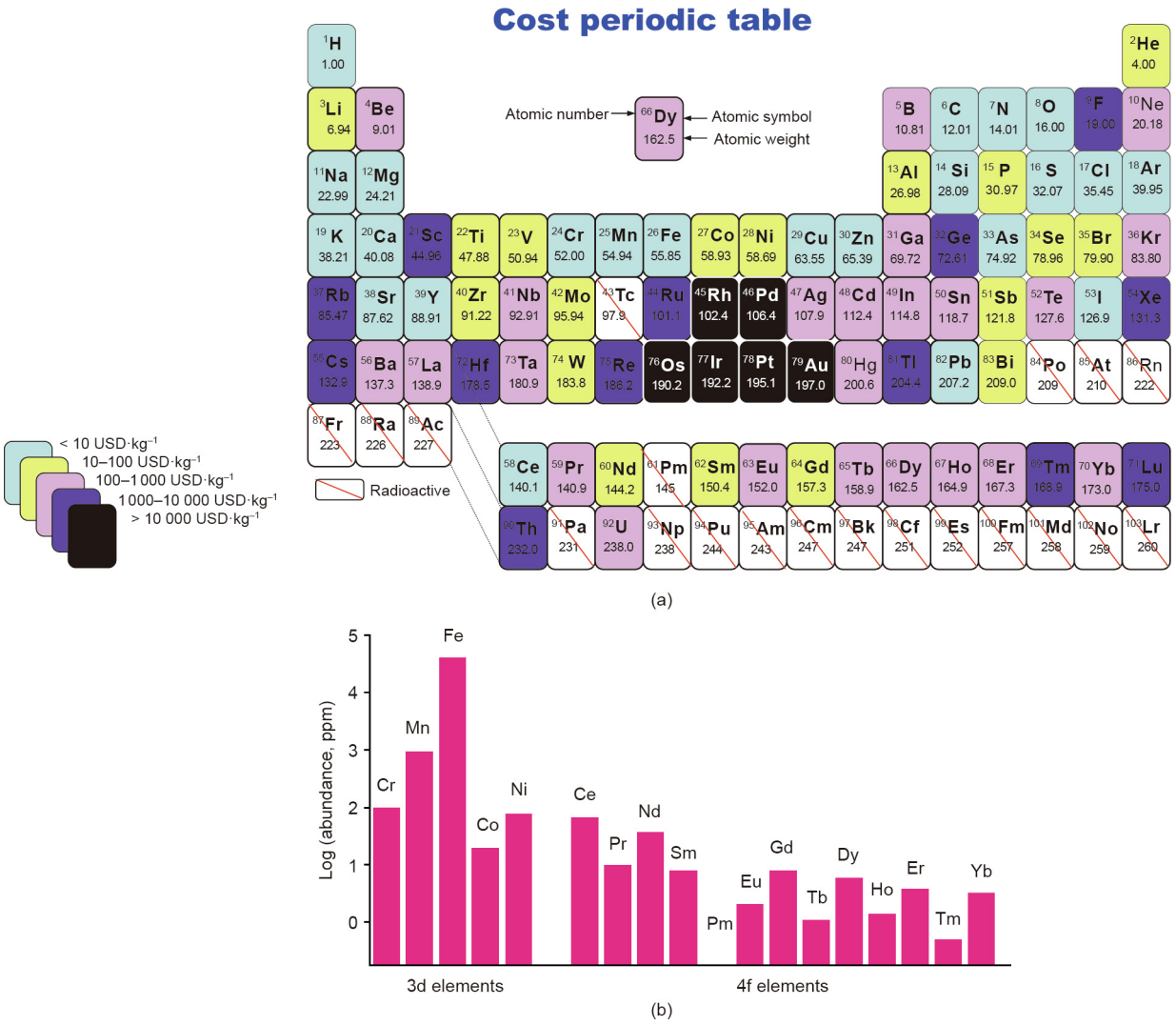

Fig. 4. (a) The periodic table of the elements assigned to five different cost categories (updated, after Ref [8]); (b) crustal abundances of magnetic elements, plotted on a logarithmic scale.

Rare earth permanent magnets are currently produced in quantities of about 1.4×10^5 t per year, with 80% of the world's supply of rare earth metals originating in China. The development of alternative sources of supply requires risky long-term investment in mines; nevertheless, some of the new prospects currently being investigated or under development in Australia, Canada, Brazil, South Africa, Vietnam, Sweden, and elsewhere will probably become significant sources of rare earth metals in future. Rare earth mining and separation is a dirty business that raises opposition from environmentalists. No rare earths are currently produced in the United States, which remains a major market for rare earth products.

Historically, the development of rare earth permanent magnets has been punctuated by supply crises for strategic raw materials. The first rare earth magnets, based on Sm–Co alloys, were discovered and developed in the late 1960s by Karl Strnat, who initiated a series of rare earth magnet workshops in 1974. At that time, "Alnicos" (i.e., Al–Ni–Co–Fe magnets) constituted another important slice of the magnet market. About 90% of the world's cobalt supply then came from Zaire, a country that was in the grip of warlords and racked by civil unrest. By 1979, cobalt prices had risen by a factor of six in two years to 72 USD·kg^{-1} (250 USD·kg^{-1} in current terms), as illustrated in Fig. 5(a). Magnet prices shot up correspondingly, triggering an intense international effort to find an alternative; this resulted in the discovery of Nd–Fe–B, the first iron-based rare earth magnet, by Masato Sagawa and John Croat in 1982.

The more recent rare earth crisis in 2011 (Fig. 5(b)) saw huge increases in the price of rare earth metals stemming from market mismanagement in China, which by then had become the dominant source of supply. Neodymium (Nd) and dysprosium (Dy) prices reached as high as 550 and 3350 USD·kg^{-1}, respectively, in current terms. This crisis jeopardized the credibility of future supplies of the heavy rare earth metals Dy and Tb, which constituted 5% by weight of the high-temperature grades of Nd–Fe–B used for electric vehicles at that time. The Dy/Nd ratio was about 0.16, which is comparable with the natural abundance ratio; however, the use of these metals doubled the raw material cost compared with magnets with no heavy rare earth metals. The situation was unsustainable, and the prompt response of the research community in developing heavy rare earth lean and free magnet grades [9,10] may have secured the future of permanent magnet traction electric vehicles.

In 2018, prices stabilized at 70 USD·kg^{-1} for Nd and 280 USD·kg^{-1} for Dy. The cobalt price is currently 70 USD·kg^{-1}, but remains volatile and has fluctuated between 20 and 110 USD·kg^{-1} over the past ten years, with spikes in 2008 and 2018.

The 1.4×10^5 t of rare earth magnets that are produced annually now account for well over half the magnet market by value

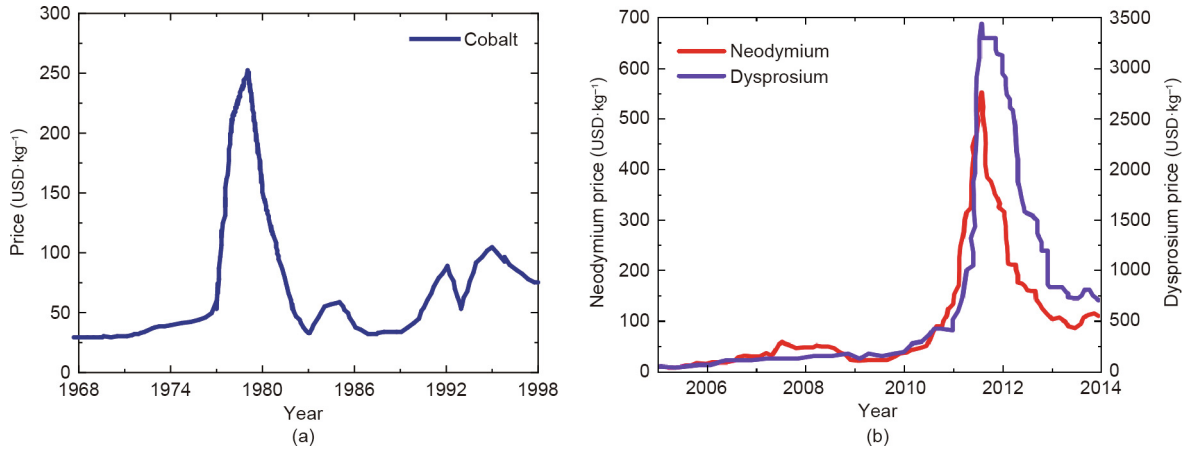

Fig. 5. Material supply crises that have shaped the development of rare earth permanent magnets. (a) Cobalt price from 1968 to 1998; (b) neodymium and dysprosium prices from 2005 to 2014.

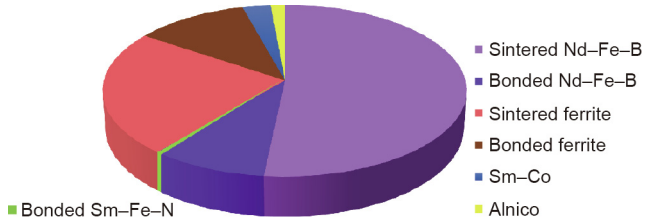

Fig. 6. Market shares for various types of permanent magnets.

(Fig. 6). The remainder are almost all hexagonal ferrites, which are produced in quantities of about 1×10^6 t per year for innumerable everyday applications. These are an order of magnitude cheaper than rare earth magnets; however, $(BH)_{MAX}$ for $BaFe_{12}O_{19}$ or $SrFe_{12}O_{19}$ is only 48 kJ·m^{-3}. Rare earth and ferrite magnets each account for roughly half of the 8 GJ of energy stored in new magnets every year.

Another stimulus has been the special specifications required for technical applications. The development of laptop computers demanded hard disc drives with a very low profile. The first Macintosh portable, introduced in 1989, weighed 7 kg with a 40 MB drive and was 10 cm thick. Terabyte hard disc drives for laptops are now 7 mm thick. The space available for the voice coil motors is very limited, which stimulated the development of Nd–Fe–B magnets with larger coercivity and energy product. Similarly, the development of traction motors for electric vehicles with an extended temperature operating window of up to 200 °C necessitated the development of Nd–Fe–B magnets with an extended operating temperature range. A balance of demand for the different rare earth metals that matches their relative abundance in the mines is advantageous. This is an area of science in which economic factors have had a critical influence on mapping the path of technical progress.

2. Materials

2.1. Hard, semi-hard, and soft materials

The family of permanent magnets includes materials that are capable of retaining a large remanent magnetization quasi-indefinitely, regardless of shape, as well as those that require assistance in the form of a reduced demagnetizing field created by an appropriate magnet shape. Surviving examples of the latter class are the Alnicos, which-like the bar and horseshoe magnets of old—need to have a special shape in order to reduce the demagnetizing field below their coercive field, and thereby retain a near-saturated value of the magnetization. Their load line, with the slope $\mu_0(1 - 1/N)$, must be steep, and the penalty is an energy product far below the ideal maximum of $(1/4)\mu_0 M_s^2$. Magnets, which can be fabricated into any desired shape, have to be made of a hard magnetic material that is capable of exhibiting a coercivity in excess of half the magnetization, and preferably exceeds the magnetization itself. The coercivity of a material is an extrinsic magnetic property. Unlike intrinsic properties such as the Curie temperature T_C, saturation magnetization M_s, and intrinsic anisotropy K_u (usually of magnetocrystalline origin), the coercivity depends on a microstructure that allows a metastable highly magnetized state to persist after saturation. The natural lowest-energy state is a multi-domain state with no net magnetization and no appreciable stray field, which is useless for permanent magnet applications. The struggle for coercivity was the story of magnet development in the 20th century. The development of a series of materials with an ever-improved energy product culminated with the discovery of the first Sm–Co magnets in the 1960s and rare earth iron magnets based on $Nd_2Fe_{14}B$ in the early 1980s. There is still no easy route to coercivity; each new material must pass through an empirical process of optimization that extends over decades. The anisotropy field $H_a = 2K_u/(\mu_0 M_s)$, which is an intrinsic property that corresponds to the reversal field for a monodomain Stoner–Wohlfarth particle, acts as a physical upper limit [6]. It usually requires many years of work to achieve a coercivity that is 20%–30% of H_a. The hardness parameter of a material κ is an empirical guide to the feasibility of such an endeavor. κ is defined in terms of the ratio of anisotropy to magnetostatic energy, as follows:

$$\kappa = \left(\frac{K_u}{\mu_0 M_s^2}\right)^{1/2} \tag{4}$$

A hard magnetic material capable of development into permanent magnets that are unconstrained by shape is defined by the following criterion:

$$\kappa > 1 \tag{5}$$

The first materials to break the shape barrier were the $L1_0$ compound CoPt [11,12] and the hexagonal ferrite $BaFe_{12}O_{19}$ [13]. Later, it was realized that rare earth elements could be excellent sources of magnetocrystalline anisotropy; all of today's high-performance permanent magnets are made from rare earth transition metal (RE–TM) intermetallic compounds such as $Nd_2Fe_{14}B$ [14–16], Sm_2Co_{17} [17], and $Sm_2Fe_{17}N_3$ [18,19].

It is worth noting that Eq. (5) is a necessary but insufficient criterion for a good permanent magnet. This criterion can be comfortably satisfied by certain materials such as α-Fe_2O_3 because they are only weakly ferromagnetic with a tiny value of M_s. Although the development of coercivity may be easy, these materials produce only a very small stray field that scales with M_s, and are useless as permanent magnets. The criterion $\kappa > 1$ must be coupled with a useful value of M_s, which can be arbitrarily set as $\mu_0 M_s > 0.4$ T.

When magnetocrystalline anisotropy is insufficient to satisfy the criterion $\kappa > 1$, it is still possible, as explained above, to make a ferromagnetic material into a magnet, albeit with a relatively poor energy product. Semi-hard materials are defined as those with $1 > \kappa > 0.1$. Provided that $\kappa \gtrsim 0.5$, permanent magnets using these materials are a possibility. Here, the Alnicos are a particularly interesting class of materials. These alloys of Al, Ni, Co, and Fe, along with other additives, possess a nanostructure of acicular nanoregions of ferromagnetic Fe–Co embedded in a nonmagnetic Al–Ni matrix. The Fe–Co is cubic, with no uniaxial magnetocrystalline anisotropy. The appropriate nanostructure is achieved by an elaborate thermal process involving spinodal decomposition. The origin of the uniaxial anisotropy in these materials can be characterized as intrinsic shape anisotropy. The elongated ferromagnetic nanoregions have a demagnetizing factor N_n. They exhibit a uniaxial anisotropy that is attributable to their shape [6], which follows Eq. (1), with

$$K_u = \frac{1}{4}\mu_0 M_s^2 (1 - 3N_n) \tag{6}$$

Inserting the maximum possible value of $(1/4)\mu_0 M_s^2$ into Eq. (4) gives $\kappa = 0.5$, which falls considerably short of the criterion in Eq. (5). In fact, the Fe–Co alloy only occupies a fraction ($f \approx 0.7$) of the magnet volume, which provides a slightly better result of $\kappa = 0.7$; however, it is unrealistic to assume that N_n can be zero for this packing fraction.

As mentioned earlier, ferromagnets with limited coercivity can be shaped in macroscopic forms such as bars and horseshoes that make use of global shape anisotropy to maintain their magnetization. This is usually what is done with semi-hard materials with $\kappa < 1$. Cobalt, Alnico, $L1_0$-FeNi, and α″-$Fe_{16}N_2$ all fall into this category. The energy product is then limited to a fraction on the order of 10% of $(BH)_{MAX}$. Many hard and semi-hard materials are included in the plot of Fig. 7. The third class of magnetic materials comprises soft materials with $\kappa < 0.1$. These exhibit little or no coercivity, and do not concern us here.

2.2. Thin films, powder, and composites

The literature often reports energy products for samples that are thin films or powders. However, these reports should be treated with caution. For powders, an approximate correction is made for the demagnetizing factor, such as $N_{eff} = 1/3 + f(N' - 1/3)$, where N' is the demagnetizing factor for the overall sample shape. The measured B is then divided by f in order to "correct" the $B(H)$ curve to the full material density (7760 kg·m^{-3} for $Nd_2Fe_{14}B$, for example) and $(BH)_{max}$ is then deduced in the normal way. Section 2.3 compares the powder energy product data for $Sm_2Fe_{17}N_3$, a material that cannot be sintered effectively because it decomposes before reaching the necessary sintering temperature, with data on bonded magnets made from this material. The magnet energy products are the more meaningful data because they show what can be expected in an application. Powder values are misleadingly optimistic.

The energy products that are sometimes cited for "thin-film permanent magnets" are even more confusing [20]. This term is actually an oxymoron, because a uniformly magnetized thin film produces no magnetic field in the surrounding space regardless of magnetization direction, except just around the edges of the film [2]. The energy product is practically zero, no matter how wide or

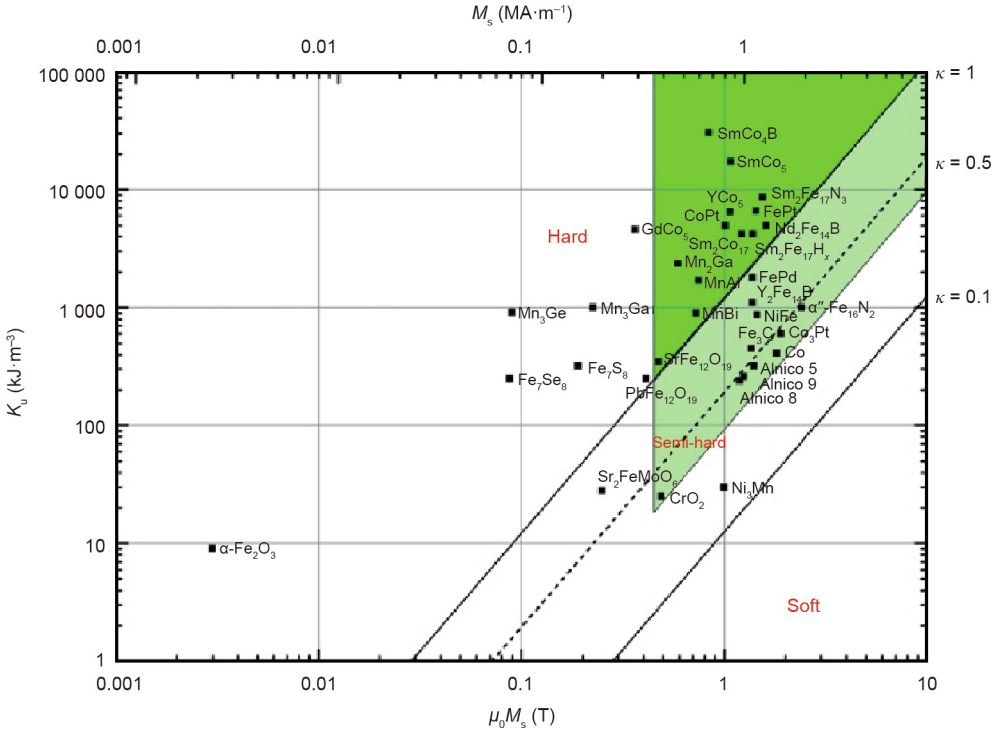

Fig. 7. Plots of anisotropy K_u as a function of polarization $\mu_0 M_s$ for many magnetic materials with uniaxial anisotropy. The anisotropy of the Alnicos is intrinsic shape anisotropy. Solid and dotted lines correspond to $\kappa = 1$, 0.5, and 0.1. Hard materials in the bright green area can be used to make efficient magnets of any shape. Semi-hard materials in the pale green area can be used to make oriented magnets with a shape-limited energy product. Reproduced from Ref. [2] with permission of Elsevier B.V., © 2015.

square the plot of M versus applied field may be [3]. This does not mean that thin films of hard magnetic materials such as Fe–Pt cannot be very useful for magnetic recording, especially when they are magnetized perpendicular to the plane. In that case, however, they are not uniformly magnetized; rather, they are patterned into regions with dimensions that are comparable to the film thickness. These regions project a stray field into the surrounding space over a distance that is comparable to their size, which can then be read by a read head close to the film surface. The dimensions of a useful permanent magnet in three orthogonal directions will always be roughly equal. However, this is surely not the case for a uniformly magnetized thin film.

Permanent magnets are skillfully engineered mixtures of phases designed to create coercivity in the major constituent, which possesses favorable intrinsic magnetic properties T_C, M_s, and K_u. An interesting approach that has been investigated for many years is to make a two-phase nanocomposite of a high-moment soft phase, exchange coupled to a high-anisotropy hard phase [21]. These exchange-spring magnets [22] should be able to average the magnetization and anisotropy of the two constituents [8]; however, in order to make an impact on the record energy product, the hard phase must be crystallographically aligned. Soft-in-hard geometries are better than hard-in-soft ones [3], especially a configuration of soft cylinders in a hard matrix [23]. The key to the approach is the quantity $(A/K_u)^{1/2}$, which is proportional to the domain wall width of the hard phase. The grand challenge is still to find a way to engineer a bulk nanocomposite on a scale where the soft regions separating the aligned hard regions are no more than about 10 nm thick. Thin films may help to prove the principle [24–27], but useful permanent magnets are bulk functional materials. There may be some promise in a recent report by Li et al. [28].

Another approach is to exploit shape anisotropy in aligned composites of semi-hard materials. The best results have been achieved with cobalt nanowires chemically grown using polyol and then aligned [29,30]. Cobalt is a semi-hard material with $(BH)_{MAX}$ = 500 kJ·m^{-3} and κ = 0.45, so substantial shape anisotropy is needed to make it into a permanent magnet. The energy product of the aligned nanowires, extrapolated to 100% density, is 350 kJ·m^{-3} [29]. Encouraging energy products of 165 kJ·m^{-3} have been reported for composites containing 54% by volume of well-aligned 22 nm Co nanorods with square hysteresis loops [30]. Warm compaction at 180 °C with no binder has led to dense, oriented nanowire arrays, but a lower energy product (65 kJ·m^{-3}) [31]. Magnetization reversal is coherent in these aligned nanowire assemblies [32], which have clear potential as gap magnets. A limitation is the thermal instability of hexagonal cobalt above 422 °C, where it transforms into the face-centered cubic structure and loses its uniaxial magnetocrystalline anisotropy. A more practical snag is that the cost of Co is now comparable to that of Nd.

2.3. Sm–Fe–N magnets

When $Sm_2Fe_{17}N_3$ was discovered in the search for even better iron-based rare earth magnets [18,19] following the discovery of $Nd_2Fe_{14}B$, this nitride appeared to offer superior magnetic properties (Curie temperature T_C, and uniaxial anisotropy K_u) or comparable magnetic properties (spontaneous magnetization M_s). The drawback was its instability. Unlike $Nd_2Fe_{14}B$, which is stable at high temperatures when boron is introduced into the melt, the samarium–iron nitride is a low-temperature phase, prepared by gas-phase interstitial modification from a Sm–Fe precursor with a Th_2Zn_{17} [18] or $TbCu_7$ [33] structure using nitrogen (N_2) or ammonia (NH_3) gas [34] at about 450 °C. The nitrogen occupies three interstitial sites surrounding the Sm [35], as shown in Fig. 8, where it creates a strong negative electric field gradient on the samarium, leading to a large positive contribution to the K_1 term in the magnetocrystalline anisotropy. Unfortunately, the nitride decomposes when heated to about 600 °C, which makes high-temperature sintering of Sm–Fe–N impossible. Attempts to circumvent this limitation by explosive or shock compression [36–38], or by spark plasma or current sintering [39–42] have met with only limited success.

Metal bonding was an early approach to forming a bulk magnet [43]. Zinc was found to be the best binder, as it melts at 420 °C and reacts with free iron to form the nonmagnetic Zn_7Fe_3 phase. Recent work has yielded dense zinc-bonded Sm–Fe–N magnets with a high coercivity (2.7 MA·m^{-1}) but modest energy products [44]. Zinc coating [45] improves powder coercivity for resin-bonded magnets. A new eutectic Sm–Fe–Cu–Al that melts at 495 °C and retains the coercivity of Sm–Fe–N powder is currently under investigation [46], with the goal of achieving dense, oriented sintered

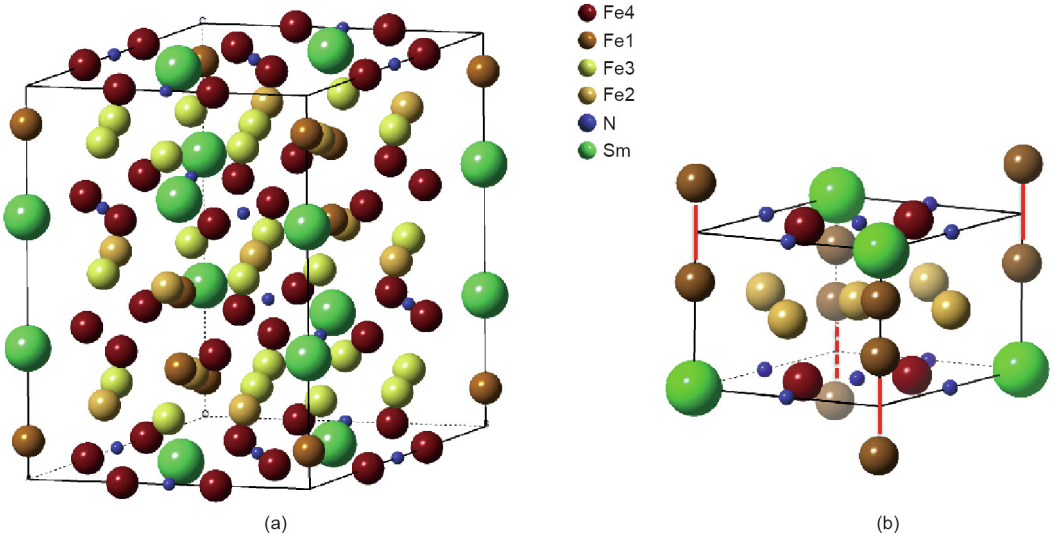

Fig. 8. (a) Rhombohedral Th_2Zn_{17} and (b) hexagonal $TbCu_7$ structures for samarium–iron nitride. The former is the structure of stoichiometric $Sm_2Fe_{17}N_3$, but the latter does not have a precisely defined composition. The Sm and Fe sites along the vertical cell edges are partially occupied in such a way that no two closely spaced adjacent sites are simultaneously occupied. A samarium atom can be replaced by a dumbbell pair of iron atoms, connected in red, more or less at random. Fe1, Fe2, Fe3, and Fe4 are different iron sites.

magnets. None of the oriented, polymer-bonded magnets that have been produced so far have energy products above 200 kJ·m^{-3}, values that are only about half those of the powder, as illustrated in Fig. 9. Improvements in the magnetic properties of the powder have been achieved by reducing the particle size [44,45,47] in order to limit the effect of nucleation centers, and by improving surface quality [48].

Melt-spun Sm–Fe alloy ribbons had already been nitrided to form hard Sm–Fe–N powder as early as 1991 [49]. It was found that a wheel speed slower than 15 m·s^{-1} yielded powder with the Th_2Zn_{17} structure, whereas faster wheel speeds yielded powder with the disordered $TbCu_7$ structure, and approximate composition $SmFe_9$ (Fig. 8(b)). This process was developed by Daido Steel, who commercialized Nitroquench powder, a product that rivals Magnequench material for isotropic bonded magnets while offering superior corrosion resistance. A new study showed that the remanence of the melt-spun material is 64% of the saturation magnetization [50], an effect that has been attributed to the nanoscale dimensions (15 nm on average) of the Sm–Fe–N crystallites. As a result, the energy product of the fully-dense coercive powder is 164 kJ·m^{-3}, which is significantly greater than a quarter of the $(BH)_{MAX}$ = 475 kJ·m^{-3} that would be anticipated if the material were isotropic.

A final point concerns the anisotropy in $Sm_2Fe_{17}N_3$. The literature value of the anisotropy constant K_1 is based on measurements in a large transverse field or else in a pulsed field, in order to determine the singular point in the time derivative of the magnetization at 14 T [4,33,50]. However, Iriyama et al. [19] have fitted data in a transverse field of 26 T, which does not quite saturate the powder, to an expression with K_1 and K_2 that yields K_1 = 6.6 MJ·m^{-3} and K_2 = 3.3 MJ·m^{-3}. They deduced an anisotropy field $\mu_0 H_a = (2K_1 + 4K_2)/M_s$ = 22 T that is indeed three times greater than that of $Nd_2Fe_{14}B$. However, the coercivity in $Sm_2Fe_{17}N_3$ is nucleation controlled, so it is the nucleation field $H_n = 2K_1/M_s$ that limits the coercivity [51]; the value is then 11 T—still greater than $Nd_2Fe_{14}B$, but not as large as was first thought.

Sm–Fe–N powders are now marketed by several other companies for anisotropic bonded magnets (e.g., Sumitomo, Nichia, Magvalley). Although production is < 1% of that of Nd–Fe–B and processing costs are still high, there are prospects for increasing market share. Although neodymium is four times more abundant, samarium is currently four times cheaper because it is regarded as a byproduct of neodymium production. A more balanced uptake of the different rare earths would eventually increase the price of samarium; but for now, samarium is a bargain.

2.4. 1:12 and other materials

A weakness of $Nd_2Fe_{14}B$ is its relatively low T_C of 315 °C, which limits the operating temperature range and introduces a much larger temperature dependence of magnetic values than is found, for example, in Alnico. The Curie temperature may be improved by cobalt substitution at the expense of weakening the net transition metal anisotropy, and the addition of a heavy rare earth to increase the anisotropy again weakens the magnetization. The best high-temperature magnets at present are based on pinning-controlled Sm_2Co_{17} compositions. It is thus a challenge to find an iron-based rare earth permanent magnet with improved high-temperature performance, whether for electric vehicle traction such as cars and trains (160–200 °C) or aerospace applications such as generators, bearings, and thrusters (up to 500 °C). Interstitial magnets containing nitrogen or carbon (but not boron) tend to decompose at around 600 °C [52].

The potential of the 1:12 phase for permanent magnet development has long been recognized [53]. The tetragonal $ThMn_{12}$ structure is related to that of $SmCo_5$ ($CaCu_5$-type) and it is obtained by replacing half of the rare earth atoms with transition metal dumbbells, as shown schematically in Fig. 8 and Fig. 10 [54]. In the 1:12 structure, there is one rare earth site (2a) at the corners of the unit cell, and three transition metal sites: 8f, 8i, and 8j. A 2b interstitial site at 0, 0, 1/2 midway between two rare earths can accommodate a small interstitial atom, N or C. The $SmFe_{12}$ compound is unstable in bulk, although it is well-known in thin films [53]. Normally, a large transition metal such as titanium (Ti) must occupy some 8i sites in order to stabilize the structure, as in $Sm(Fe_{11}Ti)$. The intrinsic magnetic properties of this alloy are compared with those of $Nd_2Fe_{14}B$ in Table 2. The magnetization, which is substantially reduced by the presence of Ti, is inferior, but the Curie temperature is higher. Simultaneous substitution of zirconium (Zr) on the Sm sites and Co on the Fe sites yields an optimized composition $(Sm_{0.8}Zr_{0.2})(Fe_{0.75}Co_{0.25})_{11.5}Ti_{0.5}$ [55], which offers superior intrinsic magnetic properties to those of $Nd_2Fe_{14}B$ (Table 2). A challenge for all 1:12 magnet development is to find an appropriate nonmagnetic intergranular phase that could be used for liquid-phase sintering.

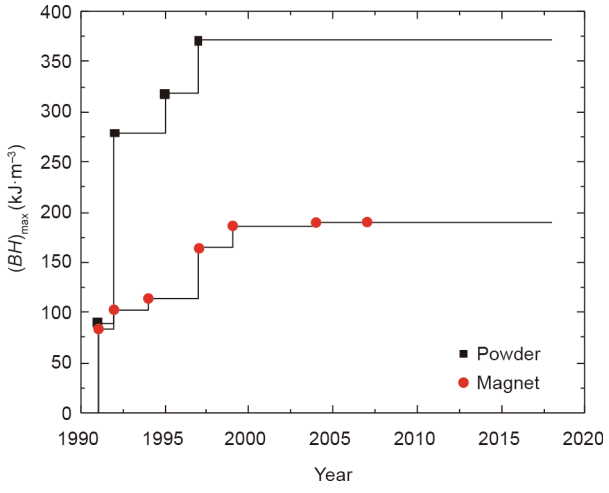

Fig. 9. Progress over time in advancing the energy products of Sm–Fe–N powders and permanent magnets.

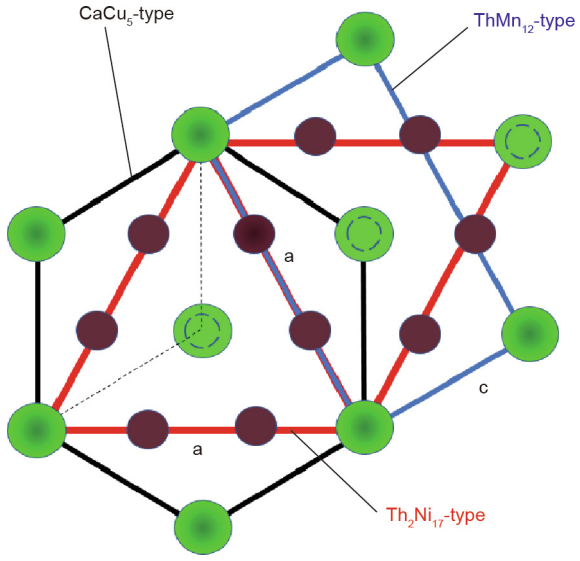

Fig. 10. Relation of the $CaCu_5$, Th_2Ni_{17}, and $ThMn_{12}$ structures [54].

Table 2
Intrinsic magnetic properties of some permanent magnet phases.

Compound	T_C (K)	$\mu_0 M_s$ (T)	K_1 (MJ·m^{-3})	κ	$(BH)_{MAX}$ (kJ·m^{-3})
$Nd_2Fe_{14}B$	588	1.61	4.3	1.54	516
$Sm_2Fe_{17}N_3$	749	1.54	8.6	2.13	472
$Sm_2Fe_{11}Ti$	590	1.21	4.0	1.85	291
$NdFe_{11}TiN$	727	1.32	4.8	1.86	347
$NdFe_{12}N$[a]	820	1.66	5.3	1.55	548
$(Sm_{0.8}Zr_{0.2})(Fe_{0.75}Co_{0.25})_{11.5}Ti_{0.5}$	800	1.63	5.9	1.67	529
$(Nd_{0.7}Zr_{0.3})(Fe_{0.75}Co_{0.25})_{11.5}Ti_{0.5}N_{0.5}$	> 730	1.68	4.0	1.33	561

K_1 is the leading term in the magnetocrystalline anisotropy and is distinct from K_u in Eq. (1), which includes a contribution from the magnetic dipole anisotropy.
[a] Thin film.

The interstitial site can be exploited to create a strong positive electric field gradient A_2^0 at the rare earth site [56], which is effective at creating uniaxial anisotropy with a rare earth such as Nd with a negative Stevens coefficient θ_2. The compound $Nd(Fe_{11}Ti)N$ [57], like $Sm_2Fe_{17}N_3$, is of interest as a hard material for oriented bonded magnets.

Although thin films are useless as permanent magnets, they can help determine the substitutions necessary to improve the intrinsic magnetic properties. Epitaxial thin films of $NdFe_{12}$ have been prepared on suitable substrates to establish the effect of Ti substitution on magnetization, and subsequently nitrided [58,59]. These films also exhibit superior intrinsic magnetic properties to those of $Nd_2Fe_{14}B$. The intrinsic properties of $Sm(Fe_{9.6}Co_{2.4})$ thin films are even better, with T_C = 586 °C, $\mu_0 M_s$ = 1.78 T, K_1 = 4.4 MJ·m^{-3}, κ = 1.32, and $(BH)_{MAX}$ = 630 kJ·m^{-3} [60]. The bulk materials have intrinsic magnetic properties that are comparable to those of Nd–Fe–B, but with Curie temperatures on the order of 500 °C [61]. In this structure, the Nd compounds need interstitial nitrogen to provide a uniaxial rare earth contribution to the anisotropy. An optimized composition is $(Nd_{0.7}Zr_{0.3})(Fe_{0.75}Co_{0.25})_{11.5}Ti_{0.5}N_{0.5}$ [62], but the stability of the nitrogen may be a limiting factor for high-temperature operation. The challenge now is to develop a microstructure that would take advantage of anisotropy fields on the order of 10 T to exhibit sufficient coercivity for these magnets to operate at 200 °C.

High-throughput computational screening for potentially useful magnetic phases using density functional theory has developed to the point at which thousands of compounds can be explored. In addition to the 1:12 structure, for which 1280 compounds have been screened by Körner et al. [63], other interesting structure types for potential rare earth magnets are 6:29, 1:13, and 1:11. A recent study of the tetragonal YNi_9In_2 structure, including possible interstitial atoms, led to a list of potentially interesting interstitial Nd–Fe-based compounds such as $Nd(Fe_{10}Co)N$ [64]. Calculated magnetization and Curie temperatures tend to be more reliable than uniaxial anisotropy constants, which may be exaggerated by as much as a factor of four. Exploration of the stability of ternary and quaternary systems is complicated by the need to explore the stability of mixtures of binary or quaternary phases on the appropriate phase diagrams, which need not be stoichiometric line compounds. Lists of the most interesting compounds produced by computational screening can readily be checked experimentally in order to determine if the compounds really exist. Experimental exploration, based on thin-film libraries or reaction crucible and reaction sintering methods [65], as well as educated intuition, are important complementary approaches.

In the search for viable new permanent magnets, affordable ingredients and useful intrinsic magnetic properties are the first and second bases. The third, and potentially toughest, base to reach is the development of an alloy microstructure that can deliver useful coercivity for the metastable fully-magnetized state (which becomes progressively more difficult with higher magnetization). Finally, there is the race to come up with a viable route to industrial production. It all takes time, persistence, and determination; in permanent magnetism, there are no home runs.

3. Processing

3.1. Nd–Fe–B magnets and rare earth content

A trend that began even before the recent rare earth crisis, and has since accelerated, has been to further optimize Nd–Fe–B magnets, especially by reducing or eliminating heavy rare earth additions [9,10]. This material is now established as dominant in the global magnet market (Fig. 6).

Part of the response has been to tailor the materials more closely to fit the applications. The heavy rare earth metals serve to increase the uniaxial anisotropy via their spin-orbit interaction. Nucleation of reverse magnetization tends to occur predominantly at surface irregularities of the hard magnetic grains, so one solution is to harden only the vulnerable surfaces and interfaces with costly Dy or Tb via a grain-boundary diffusion process [66]. Otherwise, when certain segments of a magnet in an electrical drive are subject to large second-quadrant recoil fields, it may be appropriate to enhance the coercivity of only those sections by means of Dy or Tb doping. On another level, time-variable permanent magnets or switchable permanent magnets may be achieved with appropriate magnetic circuit design.

The need for heavy rare earth metals has been reduced in recent years through fine control of the process parameters, and especially milling and the reduction of the particle size of the powders used to make Nd–Fe–B magnets to the 1 μm range. Even Nd can be used more sparingly by replacing some of it with a lattice-matched mixture of La and Ce [67,68], both of which are cheaper and more abundant elements.

The quest for new, high-performance rare earth free magnet materials to bridge the wide gap between $Nd_2Fe_{14}B$ (with $(BH)_{MAX}$ = 515 kJ·m^{-3}) and $BaFe_{12}O_{19}$ (with $(BH)_{MAX}$ = 45 kJ·m^{-3}) has been less successful [69]. Hexagonal ferrites are produced in huge quantities, around 1×10^6 t per year, and share the market with rare earth magnets, as illustrated in Fig. 6. There is an opportunity to fill this gap with a new "gap magnet," provided a material can be found that satisfies the stringent price/performance criterion of costing no more than one dollar per joule of magnetic energy. Many of the compounds that have been proposed contain other costly elements such as bismuth (Bi), gallium (Ga), or yttrium (Y) [70]. Others have inadequate anisotropy [2] (Fig. 7).

3.2. Additive manufacturing

The greatest innovation in materials engineering in recent years is three-dimensional printing (i.e., additive manufacturing), which is now widely used for prototyping and manufacturing one-off

products or small runs of objects with simple or convoluted shapes. Under computer control, the printer builds up a shape as a stack of two-dimensional layers that are sequentially deposited and consolidated from a polymeric or metallic feedstock. The layers may be made of photo-cured or thermosetting polymers, polymers loaded with ceramic or metallic powder, or metallic powder that is fused by laser melting or sintering. Methods for producing bonded magnets include binder jetting, in which each layer of magnet powder is covered with a liquid thermosetting binder and the printed body is subsequently cured in an oven. The melt extrusion method often uses filaments of premixed magnetic powder and polymeric binder as a feedstock, which is melted and extruded from a moving head to build up the layers. A variant uses pellets of the composite for large-area additive manufacturing. The polymer is usually polyamide (nylon), which is also used for injection molding, and good flow is achieved for spherical Nd–Fe–B powders with diameters of about 45 μm, which are produced by gas atomization. Other approaches are based on direct laser or e-beam melting or the sintering of layers of coercive magnet powder.

Most applications to permanent magnetism have been to manufacture polymer-bonded composites of Nd–Fe–B powder. Hexagonal ferrite has not been used because the isotropic bonded magnets are very weak, with energy products of about 5 kJ·m^{-3}. The formed piece is subsequently magnetized in the usual way. Table 3 [71–81] provides a summary of some reports on Nd–Fe–B.

This work is at an early stage, with the first reports on rare earth magnets dating from 2016. Most of the results are for isotropic, polymer-bonded magnets, which, as discussed in the introduction, are not an efficient way to make use of expensive rare earth magnet materials. The energy products do not exceed 58 kJ·m^{-3}, compared with the value of 63 kJ·m^{-3} that is cited for isotropic bonded magnets with $f = 0.7$ in Table 1. The values that have been obtained thus far for denser magnets produced by laser melting Ne–Fe–B powder are no better. It is important to find a way to introduce a powder alignment step into the additive manufacturing process.

An advantage of the method is that it is possible to produce shapes or graded variations of loading densities in polymer-bonded magnets that are designed to produce a desired stray field profile [72,76], although the magnitudes of the fields that can be produced are small, on the order of 50 kA·m^{-1}. Complex channels can be created within the magnet for cooling or other fluid flow.

However, a current grand challenge is to think of a shape that cannot be manufactured by conventional compression or injection molding, and that has a unique, potentially useful magnetic functionality. Next, a suitable magnetization process must be devised to impart the necessary three-dimensional pattern of magnetization. This could be a separate step; alternatively, *in situ* magnetic fields could be applied to align and magnetize the magnetic powder, either in a uniform direction, or in a locally variable direction with pulsed microcoils. A degree of customization of standard 3D printers is needed in order to accommodate the magnetic field generator and remove all ferromagnetic material from the vicinity of the print head. The requirements for combining an *in situ* magnetic field with the laser sintering of rare earth magnet powder are even more demanding.

In addition to the papers listed in Table 3, short reviews of the current state of the art have been published [82,83], as has some information on the additive manufacturing of Sm–Co [84], Mn–Al–C [85], and Alnico 8 [86].

3.3. High-temperature magnet conditioning

Permanent magnets are essentially metastable structures, which have a multi-domain ground state that creates little or no stray field. Heating aggravates thermal instability, and the magnets experience several kinds of flux loss on heating [87]. First are the reversible losses, which are fully recoverable upon a return to ambient temperature. These reflect the intrinsic thermodynamic behavior of the material, and cannot be avoided. Remanence and coercivity naturally decline with temperature because of the temperature dependence of M_s and K_1. Next come the irreversible losses related to changes in the fully magnetized metastable domain structure at elevated temperatures. These can be cured by remagnetizing the material at ambient temperature. Finally, there are the irredeemable losses due to changes in the chemical composition or microstructure of the coexisting phases. Effects due to oxidation or rare earth volatilization fall into this last category.

It is often the practice of suppliers of magnets destined for high-temperature operation to condition their magnets at a temperature about 50 K above the operating temperature range, in order to work out the irreversible losses so that the properties of the magnet do not degrade further. Most practical rare earth magnets are rectangular or cylindrical in shape, with effective demagnetizing factors given by formulae such as $1/(2n + 1)$ and $1/(4n/\pi^{1/2} + 1)$, where n is the ratio of height to width. The example of a cylinder with $N_{eff} = 1/2$ was illustrated in Fig. 2, where it can be seen that the demagnetizing field is particularly enhanced at the pole surfaces and corners. These areas are especially susceptible to demagnetization, which has been confirmed by domain structure observation of the ground and polished surfaces of high-temperature Sm–Co magnets [88] (Fig. 11). The magnetic damage leading to irreversible losses is concentrated in these limited regions. It was then demonstrated by Xia et al. [88] that the problem can be circumvented by conditioning the magnet at a high temperature between two slabs of soft iron, which moves the pole surfaces away from the Sm–Co magnet body. These procedures

Table 3
Rare earth permanent magnets produced by additive manufacturing.

Material	Loading/binder	Method	$\mu_0 M_r$ (T)	H_c (kA·m^{-1})	$(BH)_{max}$ (kJ·m^{-3})	Ref.
Nd–Fe–B	45%/—	Binder jetting	0.32	740	20	[71]
Nd–Fe–B	38%/polyamide	Melt extrusion	0.31	740	—	[72]
Nd–Fe–B	65%/polyamide	Melt extrusion	0.51	688	44	[73]
Nd–Fe–B	40%/epoxy	Inkjet writing	0.30	1000	—	[74]
Nd–Fe–B	43%/diethylene glycol/eutectic	Binder jetting	0.31	1345	—	[75]
Nd–Fe–B	47%/polyamide	Melt extrusion	0.31	745	15	[76]
Nd–Fe–B	83%	Laser melting	0.50			[77]
Nd–Fe–B	92%	Laser melting	0.59	695	45	[78]
Nd–Fe–B	41%/polyamide	Polymer laser melting	0.32	760	15	[79]
Nd–Fe–B	70%/polyamide	Melt extrusion	0.58	708	58	[80]
Nd–Fe–B	60%/methacrylate	Photo-polymerization	0.38	760	22	[81]

M_r: remanent magnetization; H_c: corcivity.

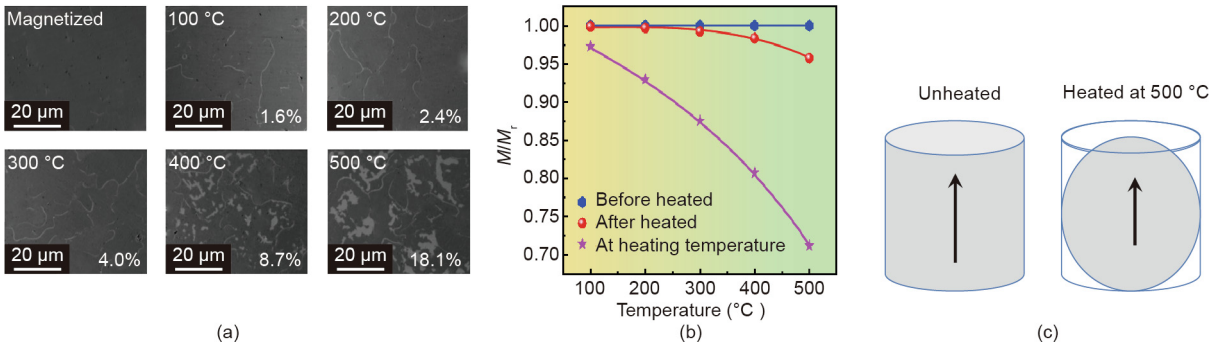

Fig. 11. (a) Domain images of the upper surface of a cylindrical Sm_2Co_{17} magnet after heating to different temperatures; (b) the relative magnetization on heating at temperatures up to 500 °C is illustrated schematically on the right; (c) the polar surfaces and edges of the cylinder are demagnetized to some extent, thereby changing the effective shape of the magnet.

may be integrated into a systems engineering approach for the optimization of stable high-temperature permanent magnet drives.

4. The future

The development of rare earth permanent magnets is at a mature stage, but is far from a spent force. As often occurs, the technology currently in place—in this case, Nd–Fe–B and Sm–Co magnets—enjoys the inbuilt advantage that it is easier to improve a technology that is established and well understood to its absolute limit, rather than to begin afresh with something new. Complementary metal–oxide semiconductor (CMOS) and hard disc recording are good examples.

Promising intermetallic systems exist in which the intrinsic magnetic properties may justify the tough struggle to develop the optimum microstructure for coercivity, and more such systems could emerge from sustained materials genomics and machine learning on other structure types. However, such exploration for bulk functional magnetic materials is inevitably subject to difficult and erratically time-varying material cost constraints. A portfolio of usable materials is an advantage, and new materials can initially be developed for a niche application in which they present a clear advantage—such as the use of melt-spun Sm–Fe–N for corrosion resistance.

Multiscale modeling is providing some physical insight into the origin of coercivity and the reasons for the still-yawning gap between optimized coercivity and the anisotropy field. At the same time, new experimental studies are uncovering information on the nanoscale grain-boundary phase, which turned out to be ferromagnetic in the case of Nd–Fe–B.

Much progress has been made toward reducing or eliminating heavy rare earths while maintaining magnet performance. However, there has been little progress toward a viable rare-earth-free gap magnet. Aligned cobalt nanowire composites are promising, but the economic case is tricky when Nd or Co prices per kilogram (or per cubic meter) are similar.

Exchange-spring magnets and additive manufacturing provide challenges, which amount in both cases to effectively orienting the hard phase. Success in either case would be a breakthrough. Encouraging progress has been made toward increasing the energy product of nanoscale exchange-spring compositions [28].

There seems to be little doubt that the rare earth magnet market will continue to expand with the rise of electric mobility and robotics, and that a balance between rare earth metal supply and demand will be achieved. More focus is anticipated on high-temperature magnet physics. In addition, there will surely be more surprises, successes, and disappointments in future. May the small store of energy in the stray field of permanent magnets, which requires no continuous energy supply to replenish it, continue to engage our curiosity and inventiveness!

Acknowledgements

This work was supported by Science Foundation Ireland as part of the ZEMS project (16/IA/4534). The following people assisted in the preparation of this manuscript: Yangkun He, Eleanor Mullen, Katarzyna Siewierka, and Jane O'Reilly.

References

[1] Coey JMD. Permanent magnets. In: Webster JG, editor. Wiley encyclopedia of electrical and electronic engineering. Hoboken: John Wiley & Sons, Inc.; 2014.
[2] Skomski R, Coey JMD. Magnetic anisotropy—how much is enough for a permanent magnet? Scr Mater 2016;112:3–8.
[3] Skomski R. Permanent magnets: history, current research, and outlook. In: Zhukov A, editor. Novel functional magnetic materials. Cham: Springer International Publishing AG; 2016. p. 359–95.
[4] Hono K, Sepehri-Amin H. Prospect for HRE-free high coercivity Nd–Fe–B permanent magnets. Scr Mater 2018;151:6–13. 154:277–283.
[5] Hu B, Rao X, Wang Y. Rare earth permanent magnet materials. 2 volumes. Beijing: Metallurgical Industry Press; 2017. Chinese.
[6] Coey JMD. Magnetism and magnetic materials. Cambridge: Cambridge University Press; 2010.
[7] Brown WF. Micromagnetics. New York: Interscience Publishers, Inc.; 1963.
[8] Coey JMD. Hard magnetic materials: a perspective. IEEE Trans Magn 2011;47 (12):4671–81.
[9] Skokov KP, Gutfleisch O. Heavy rare earth free, free rare earth and rare earth free magnets—vision and reality. Scr Mater 2018;154:289–94.
[10] Mohapatra J, Liu JP. Rare-earth-Efree permanent magnets: the past and future. In: Bruck E, editor. Handbook of Magnetic Mterials, 27. Amsterdam: Elsevier; 2018. p. 1–58.
[11] Jellinghaus W. New alloys with high coercive force. Z Tech Physik 1936;17:33–6.
[12] Klemmer T, Hoydick D, Okumura H, Zhang B, Soffa WA. Magnetic hardening and coercivity mechanisms in $L1_0$ ordered FePd ferromagnets. Scr Metall Mater 1995;33(10–11):1793–805.
[13] Kooy C, Enz U. Experimental and theoretical study of the domain configuration in thin layers of $BaFe_{12}O_{19}$. Philips Res Repts 1960;15:7–29.
[14] Sagawa M, Fujimura S, Yamamoto H, Matsuura Y, Hiraga K. Permanent magnet materials based on the rare earth–iron–boron tetragonal compounds. IEEE Trans Magn 1984;20(5):1584–9.
[15] Sagawa M, Hirosawa S, Yamamoto H, Fujimura S, Matsuura Y. Nd–Fe–B permanent magnet materials. Jpn J Appl Phys 1987;26(6):785–800.
[16] Herbst JF. $R_2Fe_{14}B$ materials: intrinsic properties and technological aspects. Rev Mod Phys 1991;63(4):819–98.
[17] Kumar K. $RETM_5$ and RE_2TM_{17} permanent magnets development. J Appl Phys 1988;63(6):R13–57.
[18] Coey JMD, Sun H. Improved magnetic properties by treatment of iron-based rare earth intermetallic compounds in ammonia. J Magn Magn Mater 1990;87 (3):L251–4.
[19] Iriyama T, Kobayashi K, Imaoka N, Fukuda T, Kato H, Nakagawa Y. Effect of nitrogen content on magnetic properties of $Sm_2Fe_{17}N_x$ ($0 < x < 6$). IEEE Trans Magn 1992;28(5):2326–31.

[20] Kalache A, Markou A, Selle S, Höche T, Sahoo R, Fecher GH, et al. Heteroepitaxial growth of tetragonal $Mn_{2.7-x}Fe_xGa_{1.3}$ ($0 \le x \le 1.2$) Heusler films with perpendicular magnetic anisotropy. APL Mater 2017;5(9):096102.
[21] Skomski R, Coey JMD. Giant energy product in nanostructured two-phase magnets. Phys Rev B Condens Matter 1993;48(21):15812–6.
[22] Kneller EF, Hawig R. The exchange-spring magnet: a new material principle for permanent magnets. IEEE Trans Magn 1991;27(4):3588–660.
[23] Jiang JS, Bader SD. Rational design of the exchange-spring permanent magnet. J Phys Condens Matter 2014;26(6):064214.
[24] Coey JMD, O'Donnell K, Qinian Q, Touchais E, Jack KH. The magnetization of $\alpha''Fe_{16}N_2$. J Phys Condens Matter 1994;6(4):L23–8.
[25] Dobosz I, Gumowska W, Czapkiewicz M. Structure and magnetic properties of Co nanowires electrodeposited into the pores of anodic alumina membranes. J Solid State Electrochem 2014;18(11):2963–72.
[26] Dumestre F, Chaudret B, Amiens C, Fromen MC, Casanove MJ, Renaud P, et al. Shape control of thermodynamically stable cobalt nanorods through organometallic chemistry. Angew Chem Int Ed Engl 2002;41(22):4286–9.
[27] Harris VG, Chen Y, Yang A, Yoon S, Chen Z, Geiler AL, et al. High coercivity cobalt carbide nanoparticles processed via polyol reaction: a new permanent magnet material. J Phys D Appl Phys 2010;43(16):165003.
[28] Li X, Lou L, Song W, Huang G, Hou F, Zhang Q, et al. Novel bimorphological anisotropic bulk nanocomposite materials with high energy products. Adv Mater 2017;29(16):1606430.
[29] Gandha K, Elkins K, Poudyal N, Liu X, Liu JP. High energy product developed from cobalt nanowires. Sci Rep 2014;4(1):5345.
[30] Anagnostopoulou E, Grindi B, Lacroix LM, Ott F, Panagiotopoulos I, Viau G. Dense arrays of cobalt nanorods as rare-earth free permanent magnets. Nanoscale 2016;8(7):4020–9.
[31] Ener S, Anagnostopoulou E, Dirba I, Lacroix LM, Ott F, Blon T, et al. Consolidation of cobalt nanorods: a new route for rare-earth free nanostructured permanent magnets. Acta Mater 2018;145:290–7.
[32] Gandha K, Mohapatra J, Liu JP. Coherent magnetization reversal and high magnetic coercivity in Co nanowire assemblies. J Magn Magn Mater 2017;438:41–5.
[33] Katter M, Wecker J, Schultz L, Grössinger R. Magnetocrystalline anisotropy of $Sm_2Fe_{17}N_2$. J Magn Magn Mater 1990;92(1):L14–8.
[34] Skomski R. Interstitial modification. In: Coey JMD, editor. Rare-earth iron permanent magnets. Oxford: Clarendon Press; 1996. p. 178–217.
[35] Miraglia S, Soubeyroux JL, Kolbeck C, Isnard O, Fruchart D, Guillot M. Structural and magnetic properties of ternary nitrides $R_2Fe_{17}N_x$ (R ≡ Nd, Sm). J Less Common Met 1991;171(1):51–61.
[36] Chiba A, Hokamoto K, Sugimoto S, Kozuka T, Mori A, Kakimoto E. Explosive consolidation of Sm–Fe–N and Sm–Fe–N/(Ni, Co) magnetic powders. J Magn Magn Mater 2007;310(2):e881–3.
[37] Hu BP, Rao XL, Xu JM, Liu GC, Wang YZ, Dong XL, et al. Magnetic properties of sintered $Sm_2Fe_{17}N_y$ magnets. J Appl Phys 1993;74(1):489–94.
[38] Chiba A, Ooyabu K, Morizono Y, Maeda T, Sugimoto S, Kozuka T, et al. Shock consolidation of Sm–Fe–N magnetic powders and magnetic properties. Mater Sci Forum 2004;449–452:1037–40.
[39] Zhang DT, Yue M, Zhang JX. Study on bulk $Sm_2Fe_{17}N_x$ sintered magnets prepared by spark plasma sintering. Powder Metall 2007;50(3):215–8.
[40] Saito T. Consolidation of Sm_5Fe_{17} powder by spark plasma sintering method. Mater Sci Eng B 2008;150(1):38–42.
[41] Saito T. Magnetic properties of Sm–Fe–N anisotropic magnets produced by magnetic-field-assisted spark plasma sintering. Mater Sci Eng B 2010;167(2):75–9.
[42] Saito T, Deguchi T, Yamamoto H. Magnetic properties of Sm–Fe–N bulk magnets produced from Cu-plated Sm–Fe–N powder. AIP Adv 2017;7(5):056204.
[43] Otani Y, Moukarika A, Sun H, Coey JMD, Devlin E, Harris IR. Metal bonded $Sm_2Fe_{17}N_{3-\delta}$ magnets. J Appl Phys 1991;69(9):6735–7.
[44] Matsuura M, Shiraiwa T, Tezuka N, Sugimoto S, Shoji T, Sakuma N, et al. High coercive Zn-bonded Sm–Fe–N magnets prepared using fine Zn particles with low oxygen content. J Magn Magn Mater 2018;452:243–8.
[45] Noguchi K, Machida K, Yamamoto K, Nishimura M, Adachi G. High-performance resin-bonded magnets produced from zinc metal-coated $Sm_2(Fe_{0.9}Co_{0.1})_{17}N_x$ fine powders. Appl Phys Lett 1999;75(11):1601–3.
[46] Otogawa K, Takagi K, Asahi T. Consolidation of $Sm_2Fe_{17}N_3$ magnets with Sm-based eutectic alloy binder. J Alloys Compd 2018;746:19–26.
[47] Kobayashi K, Skomski R, Coey JMD. Dependence of coercivity on particle size in $Sm_2Fe_{17}N_3$ powders. J Alloys Compd 1995;222(1–2):1–7.
[48] Ishikawa T, Yokosawa K, Watanabe K, Ohmori K. Modified process for high-performance anisotropic $Sm_2Fe_{17}N_3$ magnet powder. J Phys Conf Ser 2011;266(1):012033.
[49] Katter M, Wecker J, Schultz L. Structural and hard magnetic properties of rapidly solidified Sm–Fe–N. J Appl Phys 1991;70(6):3188–96.
[50] Coey JMD, Stamenov P, Porter SB, Venkatesan M, Zhang R, Iriyama T. Sm–Fe–N revisited; remanence enhancement in melt-spun Nitroquench material. J Magn Magn Mater 2019;480:186–92.
[51] Brown WF. Virtues and weaknesses of the domain concept. Rev Mod Phys 1945;17(1):15–9.
[52] Hono K. Rare earth permanent magnets with ultimate hard magnetic properties [abstract]. In: Proceedings of 2018 IEEE International Magnetics Conference (INTERMAG); 2018 Apr 23–27; Singapore. Piscataway: IEEE; 2018. p. 829.
[53] Gabay AM, Hadjipanayis GC. Recent developments in RFe_{12}-type compounds for permanent magnets. Scr Mater 2018;154:284–8.
[54] Hirosawa S, Nishino M, Miyashita S. Perspectives for high performance permanent magnets: applications, coercivity, and new materials. Adv Nat Sci Nanosci Nanotechnol 2017;8(1):013002.
[55] Kuno T, Suzuki S, Urushibata K, Kobayashi K, Sakuma N, Yano M, et al. $(Sm,Zr)(Fe,Co)_{11.0-11.5}Ti_{1.0-0.5}$ compounds as new permanent magnet materials. AIP Adv 2016;6(2):025221.
[56] Coey JMD, Otani Y, Sun H, Hurley DPF. Magnetic properties of interstitial compounds $Sm(Fe_{11}Ti)X_{1-\delta}$ (X = N, C). J Magn Soc Jpn 1991;15(4):769–72.
[57] Yang YC, Zhang X, Ge S, Pan Q, Kong L, Li H, et al. Magnetic and crystallographic properties of novel Fe-rich rare-earth nitrides of the type $RTiFe_{11}N_{1-\delta}$. J Appl Phys 1991;70(10):6001–5.
[58] Hirayama Y, Takahashi YK, Hirosawa S, Hono K. $NdFe_{12}N_x$ hard-magnetic compound with high magnetization and anisotropy field. Scr Mater 2015;95:70–2.
[59] Sato T, Ohsuna T, Yano M, Kato A, Kaneko Y. Permanent magnetic properties of $NdFe_{12}N_x$ sputtered films epitaxially grown on V buffer layer. J Appl Phys 2017;122(5):053903.
[60] Hirayama Y, Takahashi YK, Hirosawa S, Hono K. Intrinsic hard magnetic properties of $Sm(Fe_{1-x}Co_x)_{12}$ compound with the $ThMn_{12}$ structure. Scr Mater 2017;138:62–5.
[61] Tozman P, Sepehri-Amin H, Takahashi YK, Hirosawa S. Hono K. Intrinsic magnetic properties of $Sm(Fe_{1-x}Co_x)_{11}Ti$ and Zr-substituted $Sm_{1-y}Zr_y(Fe_{0.8}Co_{0.2})_{11.5}Ti_{0.5}$ compounds with $ThMn_{12}$ structure toward the development of permanent magnets. Acta Mater 2018;153:354–63.
[62] Suzuki S, Kuno T, Urushibata K, Kobayashi K, Sakuma N, Washio K, et al. A $(Nd,Zr)(Fe,Co)_{11.5}Ti_{0.5}N_x$ compound as a permanent magnet material. AIP Adv 2014;4(11):117131.
[63] Körner W, Krugel G. Elsässer C Theoretical screening of intermetallic $ThMn_{12}$-type phases for new hard-magnetic compounds with low rare earth content. Sci Rep 2016;6:24686.
[64] Körner W, Krugel G, Urban DF, Elsässer C. Screening of rare-earth-lean intermetallic 1-11 and 1-11-X compounds of YNi_9In_2-type for hard-magnetic applications. Scr Mater 2018;154:295–9.
[65] Goll D, Loeffler R, Hohs D, Schneider G. Reaction sintering as a high-throughput approach for magnetic materials development. Acta Met 2018;146:355–61.
[66] Loewe K, Benke D, Kübel C, Lienig T, Skokov KP, Gutfleisch O. Grain boundary diffusion of different rare earth elements in Nd–Fe–B sintered magnets by experiment and FEM simulation. Acta Mater 2017;124:421–9.
[67] Hussain M, Zhao LZ, Zhang C, Jiao DL, Zhong XC, Liu ZW. Composition-dependent magnetic properties of melt-spun La or/and Ce substituted nanocomposite NdFeB alloys. Phys B 2016;483:69–74.
[68] Rao X, Niu E, Du F, Hu B. Effect of cerium on magnetic properties of sintered R–Fe–B permanent magnet. [abstract]. Proceedings of 2018 IEEE International Magnetics Conference (INTERMAG); 2018 Apr 23–27; Singapore, Singapore. Piscataway: IEEE; 2018.
[69] Kuzmin MD, Skokov KP, Jian H, Radulov I, Gutfleisch O. Towards high-performance permanent magnets without rare earths. J Phys Condens Matter 2014;26(6):064205.
[70] Coey JMD. Permanent magnets: plugging the gap. Scr Mater 2012;67(6):524–9.
[71] Paranthaman MP, Shafer CS, Elliott AM, Siddel DH, McGuire MA, Springfield RM, et al. Binder jetting: a novel NdFeB bonded magnet fabrication process. JOM 2016;68(7):1978–82.
[72] Huber C, Abert C, Bruckner F, Groenefeld M, Muthsam O, Schuschnigg S, et al. 3D print of polymer bonded rare-earth magnets, and 3D magnetic field scanning with an end-user 3D printer. Appl Phys Lett 2016;109(16):162401.
[73] Li L, Tirado A, Nlebedim IC, Rios O, Post B, Vlastimil K, et al. Big area additive manufacturing of high performance bonded NdFeB magnets. Sci Rep 2016;6:36212.
[74] Compton BG, Kemp JW, Novikov TV, Pack RC, Nlebedim CI, Duty CE, et al. Direct-write 3D printing of NdFeB bonded magnets. Mater Manuf Process 2018;33(1):109–13.
[75] Li L, Tirado A, Conner BS, Chi MF, Elliott AM, Rios O, et al. A novel method combining additive manufacturing and alloy infiltration for NdFeB bonded magnet fabrication. J Magn Magn Mater 2017;438:163–7.
[76] Huber C, Abert C, Bruckner F, Groenefeld M, Schuschnigg S, Teliban I, et al. 3D printing of polymer-bonded rare-earth magnets with a variable magnetic compound fraction for a predefined stray field. Sci Rep 2017;7(1):9419.
[77] Kolb B, Huber F, Akbulut B, Donocik C, Urban N, Maurer D, et al. Laser beam melting of NdFeB for the production of rare-earth magnets. In: Proceedings of the 6th International Electric Drives Production Conference; 2016 Nov 30–Dec 1; Nuremberg, Germany. Piscataway: IEEE; 2016. p. 34–40.
[78] Jaćimović J, Binda F, Herrmann LG, Greuter F, Genta J, Calvo M, et al. Net shape 3D printed NdFeB permanent magnet. Adv Elec Mater 2017;19(8):1700098.
[79] Baldissera AB, Pavez P, Wendhausen PAP, Ahrens CH. Mascheroni JM. Additive manufacturing of bonded Nd–Fe–B—effect of process parameters on magnetic properties. IEEE Trans Magn 2017;53(11):7948722.
[80] Li L, Jones K, Sales B, Pries JL, Nlebedim IC, Jin K, et al. Fabrication of highly dense isotropic Nd–Fe–B nylon bonded magnets via extrusion-based additive manufacturing. Addit Manuf 2018;21:495–500.
[81] Shen A, Bailey CP, Ma AWK, Dardona S. UV-assisted direct write of polymer-bonded magnets. J Magn Magn Mater 2018;462:220–5.

[82] Li L, Post B, Kunc V, Elliott AM, Paranthaman MP. Additive manufacturing of near-net-shape bonded magnets: prospects and challenges. Scr Mater 2017;135:100–4.
[83] Popov V, Koptyug A, Radulov I, Maccari F, Muller G. Prospects of additive manufacturing of rare-earth and non-rare-earth permanent magnets. Proc Manuf 2018;21:100–8.
[84] Khazdozian HA, Manzano JS, Gandha K, Slowing II, Nlebedim IC. Recycled Sm–Co bonded magnet filaments for 3D printing of magnets. AIP Adv 2018;8(5):056722.
[85] Palmero EM, Rial J, de Vicente J, Camarero J, Skårman B, Vidarsson H, et al. Development of permanent magnet MnAlC/polymer composites and flexible filament for bonding and 3D-printing technologies. Sci Technol Adv Mater 2018;19(1):465–73.
[86] White EMH, Kassen AG, Simsek E, Tang W, Ott RT, Anderson IE. Net shape processing of alnico magnets by additive manufacturing. IEEE Trans Magn 2017;53(11):1–6.
[87] Cullity BD, Graham CD. Introduction to magnetic materials. Piscataway: Wiley-IEEE Press; 2008.
[88] Xia W, He Y, Huang H, Wang H, Shi X, Zhang T, et al. Initial irreversible losses and enhanced high-temperature performance of rare-earth permanent magnets. Adv Funct Mater 2019;24:19000690.